JCI insight

RESEARCH ARTICLE

Attached stratified mucus separates bacteria from the epithelial cells in COPD lungs

Joan Antoni Fernández-Blanco,[1,2] Dalia Fakih,[1] Liisa Arike,[1] Ana M. Rodríguez-Piñeiro,[1] Beatriz Martínez-Abad,[1] Elin Skansebo,[1] Sonya Jackson,[2] James Root,[2] Dave Singh,[3] Christopher McCrae,[2] Christopher M. Evans,[4] Annika Åstrand,[2] Anna Ermund,[1] and Gunnar C. Hansson[1]

[1]Department of Medical Biochemistry, University of Gothenburg, Gothenburg, Sweden. [2]Bioscience, Respiratory, Inflammation and Autoimmunity, IMED Biotech Unit, AstraZeneca Gothenburg, Gothenburg, Sweden. [3]Medicines Evaluation Unit, University of Manchester, Manchester, United Kingdom. [4]University of Colorado Denver School of Medicine, Aurora, Colorado, USA.

The respiratory tract is normally kept essentially free of bacteria by cilia-mediated mucus transport, but in chronic obstructive pulmonary disease (COPD) and cystic fibrosis (CF), bacteria and mucus accumulates instead. To address the mechanisms behind the mucus accumulation, the proteome of bronchoalveolar lavages from COPD patients and mucus collected in an elastase-induced mouse model of COPD was analyzed, revealing similarities with each other and with the protein content in colonic mucus. Moreover, stratified laminated sheets of mucus were observed in airways from patients with CF and COPD and in elastase-exposed mice. On the other hand, the mucus accumulation in the elastase model was reduced in Muc5b-KO mice. While mucus plugs were removed from airways by washing with hypertonic saline in the elastase model, mucus remained adherent to epithelial cells. Bacteria were trapped on this mucus, whereas, in non–elastase-treated mice, bacteria were found on the epithelial cells. We propose that the adherence of mucus to epithelial cells observed in CF, COPD, and the elastase-induced mouse model of COPD separates bacteria from the surface cells and, thus, protects the respiratory epithelium.

Introduction

Stagnant mucus is a problem in several airway diseases including chronic obstructive pulmonary disease (COPD) (1), cystic fibrosis (CF) (2), and asthma (3). COPD is a global health issue estimated to be the third-leading cause of death worldwide by 2020, and it is an increasing economic and personal burden. COPD is characterized by restricted airflow and progressive loss of lung function, and it encompasses 2 major phenotypes, chronic bronchitis and emphysema, both caused by an excessive inflammatory response to environmental noxious insults. Chronic bronchitis involves an increase in goblet cell number, enlarged submucosal glands, mucus hypersecretion and plugging of the airways, and chronic cough (4). Even COPD patients without chronic bronchitis have mucus obstruction of the small airways (5).

The mucociliary system keeps the bacterial numbers in the respiratory tract low and removes any inhaled particulate matter. Healthy mucus traps microorganisms and particles that are transported to the larynx, resulting in efficient cleaning. In numerous lung diseases, including COPD and CF, mucus stagnates and accumulates in the airways, leading to bacterial colonization, airway inflammation, tissue destruction, and ultimately respiratory failure. The mechanisms of mucociliary dysfunction include the aberrant overproduction of mucus, leading to accumulation on the airway surfaces. Mucus is formed by many different components, but mucins are the major macromolecular constituents. In human and pig airways, there are 2 major gel-forming mucins, the MUC5B, largely produced by glands, and the MUC5AC, secreted from the surface goblet cells. The glands form MUC5B mucin bundles that, under normal conditions, sweep the tracheobronchial surface to remove debris and bacteria (6, 7). In rodents, with few submucosal glands, both Muc5b and Muc5ac mucins are made by the surface goblet cells. Also in rodents, the Muc5b mucin is essential for keeping the mouse lungs clean under normal conditions (8).

Conflict of interest: DS has received sponsorship to attend international meetings, honoraria for lecturing or attending advisory boards, and research grants from various pharmaceutical companies including Apellis, AstraZeneca, Boehringer Ingelheim, Chiesi, Cipla, Genentech, GlaxoSmithKline, Glenmark, Johnson and Johnson, Mundipharma, Novartis, Peptinnovate, Pfizer, Pulmatrix, Skypharma, Teva, Therevance, and Verona. SJ, JR, CMC, and AÅ hold share options in AstraZeneca.

Submitted: March 8, 2018
Accepted: July 31, 2018
Published: September 6, 2018

Reference information:
JCI Insight. 2018;3(17):e120994.
https://doi.org/10.1172/jci.insight.120994.

There are several rodent models of chronic airway disease, such as induced by ovalbumin (9), IL-13 (10), LPS instillation, or cigarette smoke (11). Airway instillation of various forms of elastase, for example neutrophil elastase or porcine pancreatic elastase (PPE), has been widely used in mice, rats, guinea pigs, dogs, and ferrets as models of COPD and emphysema (12, 13). This model can be also extended to CF, since neutrophils accumulate in CF lungs (14). Based on the importance of elastase in chronic lung diseases and the fast onset of goblet cell hyperplasia (increased numbers of filled goblet cells), we have used the elastase model, where elastase was instilled i.n. twice with a 7-day interval. We have analyzed this model for goblet cell hyperplasia, mucus accumulation, and inflammation. The rodent model mucus proteome was identified and compared with that of human COPD and with colonic mucus. The importance of the Muc5ac and Muc5b mucins was addressed by using KO mice. We tested a common treatment for mucus accumulation in the airways, hypertonic saline, and its ability to detach the accumulated mucus from the epithelium. Collectively, our results show a striking similarity between the mucus accumulated in the respiratory tract of mice and COPD patients and the mucus found in the mouse and human colon.

Results

Proteome of human COPD bronchoalveolar lavage fluid. To understand the human disease COPD, we studied human bronchoalveolar lavage fluid (BALF) from never-smokers, asymptomatic smokers, and COPD patients by mass spectrometry–based (MS-based) proteomics (Supplemental Table 1; supplemental material available online with this article; https://doi.org/10.1172/jci.insight.120994DS1). Proteomic analyses revealed fewer proteins in the never-smoker group as compared with asymptomatic smokers and COPD patients (Figure 1A and Supplemental Table 2). Principal component analysis (PCA) showed a tight cluster for the never-smokers and a slightly larger cluster for the asymptomatic smokers (Figure 1B). Interestingly, the COPD patients were distributed over the entire plot, implying a large variation among individuals. Absolute quantification of a subset of mucus-related proteins revealed increased amounts of AGR2, DMBT1, FCGBP, PSCA, TFF3, TGM2, and ZG16B in COPD patients and a tendency toward increased levels of these proteins in asymptomatic smokers (Figure 1C, Supplemental Figure 1, Supplemental Figure 2, and Supplemental Table 3). The mucins MUC5AC and MUC5B were, as expected, increased in COPD patients and the ratio of MUC5AC/MUC5B changed from 0.3 in never-smokers to closer to 1.5 in asymptomatic smokers and 0.5 in COPD patients (Figure 1D).

Elastase exposure causes goblet cell hyperplasia and airway plugging. To obtain a model for COPD, mice were i.n. exposed to PPE or saline as control. The mice exposed to saline largely lacked Alcian blue/Periodic acid-Schiff–positive (AB/PAS-positive) cells in the airways, whereas a marked increase in AB/PAS-positive cells within the bronchi and bronchioles was observed in elastase-exposed mice, but not after treatment with inactivated elastase (Figure 2, A–D, and Supplemental Figure 3). Whole mouse lungs stained with AB/PAS showed that the hyperplasia had a patchy distribution, affecting bronchi and proximal bronchioles with both goblet cell hyperplasia and mucus plugging (Figure 2, C and D, and Supplemental Figure 4). This was further illustrated by transmission electron microscopy (Supplemental Figure 5A). Histopathology evaluation of inflated lungs from elastase-exposed mice revealed a mild perivascular and peribronchiolar lymphocytic inflammation relative to control mice (Figure 2E and Supplemental Figure 5B). These alterations were accompanied by a patchy damage of the septa between the alveoli, with moderate to severe multifocal loss of tissue structure as observed in emphysema. Mucus obstruction was quantified in AB/PAS-stained sections as a percentage of airway obstruction, showing a clear increase in elastase-exposed mice (Figure 2F), where the relatively smaller airways were more prone to develop severe mucus obstruction (Supplemental Figure 4). However, airways smaller than 50 μm were not affected. BALF from elastase-exposed mice showed higher immune cell counts, with a 16-fold increase in the total number of white blood cells (WBCs), consisting of increased amounts of neutrophils, eosinophils, macrophages/monocytes, and lymphocytes (Figure 2G). The increased number of inflammatory cells was accompanied by increased levels of cytokines, chemoattractants, chemokines, and EGF (Supplemental Figure 5C). In summary, i.n. elastase caused an increase in goblet cell numbers, mucus accumulation, and immune cell infiltration, as observed in human COPD.

Proteome of mouse BALF and mucus plugs. Total BALF samples collected from saline- or elastase-induced mice were analyzed by MS-based proteomics. To remove cells from BALF, samples were centrifuged, and the supernatants (SNs) were analyzed. We observed 349 proteins in controls and 408 in elastase-exposed animals (Figure 3 and Supplemental Table 4). Some of the major proteins, including

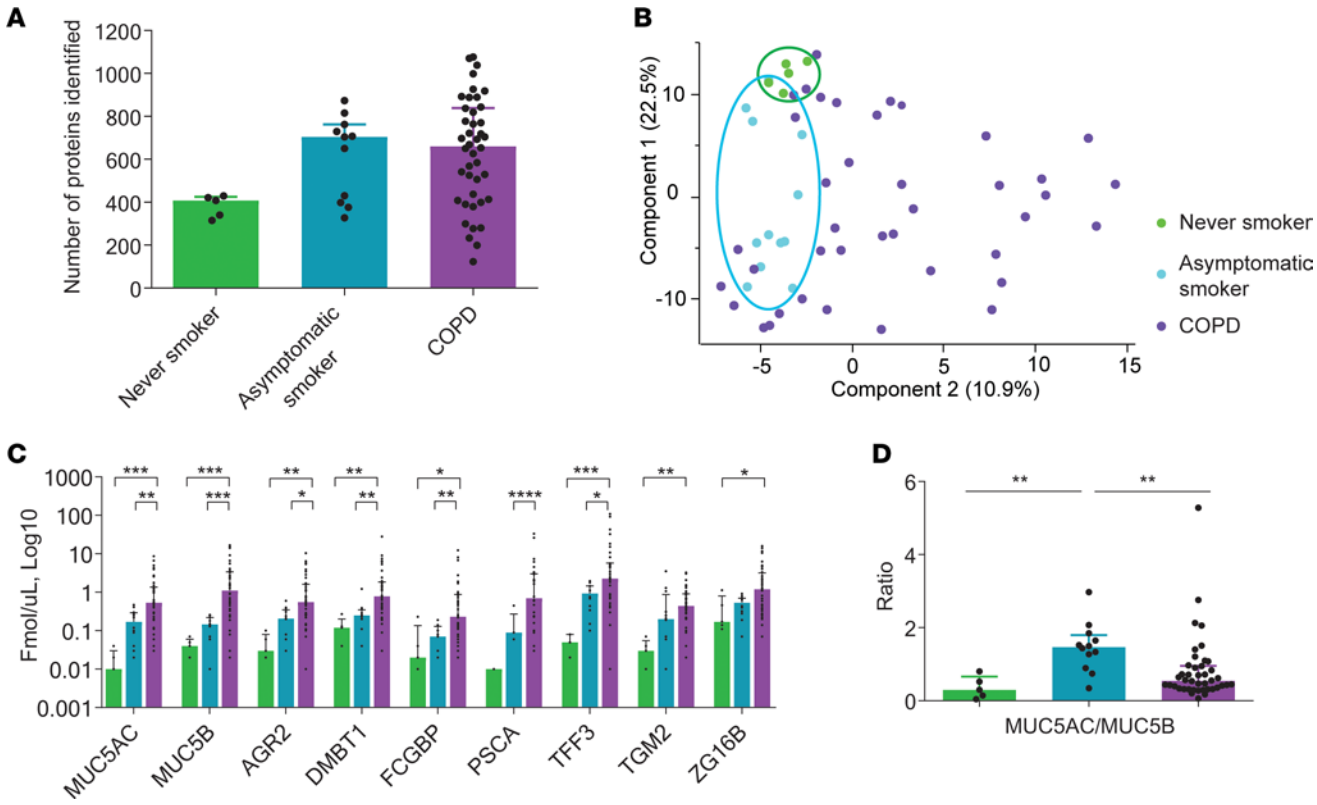

Figure 1. Altered proteome in BALF from never-smokers, asymptomatic smokers, and chronic obstructive pulmonary disease (COPD) patients. (**A**) Number of proteins identified in BALF in each sample group, never-smokers (n = 5), smokers (n = 12), and COPD (n = 42); data presented as medians ± IQR. (**B**) Principal component analysis. (**C**) Absolute quantification with isotopically labeled peptides by mass spectrometry, n = 5–42; data presented as medians ±IQR, $^{*}P \le 0.05$, $^{**}P \le 0.01$, $^{***}P \le 0.001$, $^{****}P \le 0.0001$, Kruskal-Wallis and Dunn's multiple comparisons test. (**D**) Ratio of MUC5AC to MUC5B calculated from absolute quantification data in **C**, n = 5–42 patients/group; data presented as medians ± IQR, $^{**}P \le 0.01$, Kruskal-Wallis and Dunn's multiple comparisons test. AGR2, anterior gradient protein 2; DMBT1, deleted in malignant brain tumors 1; FCGBP, Fc fragment of IgG binding protein; PSCA, prostate stem cell antigen; TFF3, trefoil factor 3; TGM2, transglutaminase-2; ZG16B, zymogen granule protein 16 B.

the club cell secreted protein uteroglobin (Scgb1a1), serotransferrin (Tf), and α-1-antitrypsin (Serpin1ad), were common for saline- and elastase-exposed mice, whereas a relative increase in mucus-related proteins, including Clca1 and chitinase-like proteins Chi3l3 and Chi3l4, were observed in the elastase-exposed mice (Figure 4, A and B). Absolute quantification of the gel-forming mucins Muc5b and Muc5ac corroborated the observed goblet cell hyperplasia, which led to Muc5ac (not detected in controls) reaching concentrations similar to those of Muc5b (Figure 4C and Supplemental Table 5). Muc5b levels were increased 24-fold compared with basal conditions. To better understand the proteins induced by elastase, we isolated mucus plugs from BALF after staining with AB (Figure 4D). The major components of the airway plugs were similar to those of the BALF but had an even higher relative level of Clca1 (Figure 3 and Figure 4E, and Supplemental Table 6). In addition, the plugs also contained high proportions of the Bpifb1 (also known as Lplunc1), Muc5ac, Muc5b, and Fcgbp. Absolute quantification of Muc5ac and Muc5b in the plugs revealed significantly higher levels of Muc5b relative to Muc5ac, in contrast with the BALF of elastase-exposed mice, where more similar levels were found (Figure 4F). In the mouse model, Clca1 was one of the most induced proteins but was absent in human BALF. In summary, the human COPD BALF showed large similarities with the elastase-exposed mice.

Proteome of isolated mouse airway epithelial cells. To further illustrate the elastase effect, we isolated airway epithelial cells and analyzed their proteome (Figure 3 and Supplemental Table 7). The epithelial cells were effectively removed as shown by mouse lung sections stained with H&E before and after epithelial removal (Figure 5A). The released cells were further purified by removing $CD45^{+}$ cells (leukocytes) and $Ly\text{-}6G^{+}$ cells (neutrophils), giving >80% $EPCAM^{+}$ cells (Supplemental Figure 6). Heatmap clustering of the proteomic results showed that the epithelial cells of elastase-exposed mice were clearly separated from the controls, with the most noteworthy differences around the Muc5b and Muc5ac (Figure 5B). Chi3l4 and Clca1 were among

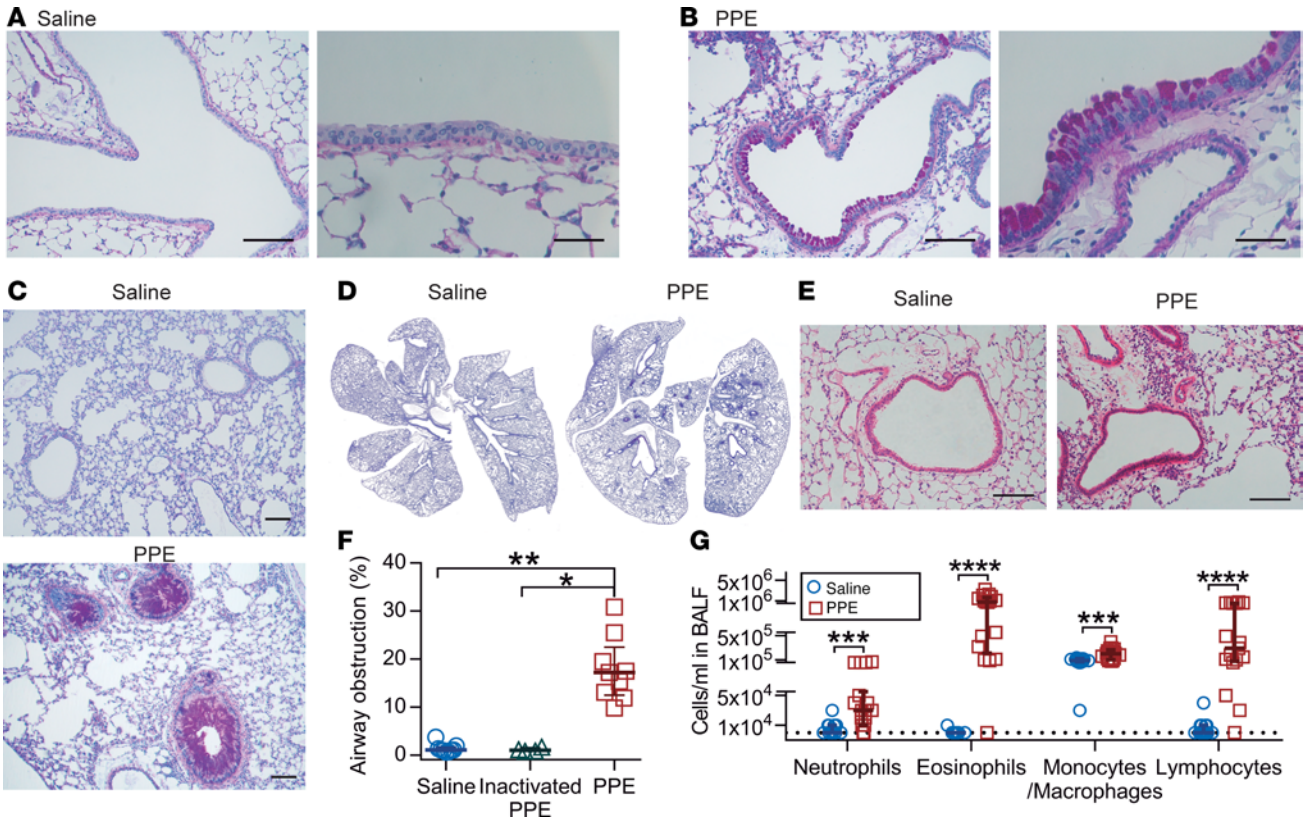

Figure 2. Mice exposed to elastase (PPE) show goblet cell hyperplasia/metaplasia and mucus accumulation in the airways. (**A**) Alcian blue/Periodic acid-Schiff–stained (AB/PAS-stained) tissue section of mice airways exposed i.n. to saline (vehicle). (**B**) AB/PAS-stained tissue section of mice airways exposed i.n. to elastase (PPE), showing a marked increase in AB/PAS-positive cells. Representative images of 4–5 animals/group. Scale bar: 100 μm (left panels) or 33 μm (right panels). (**C** and **D**) High- and low-magnification images of lungs from mice exposed to saline or elastase (PPE). Scale bar: 100 μm. (**E**) Paraffin sections stained with H&E revealed few immune cells around intrapulmonary airways and intact alveoli from saline-instilled mice. Mild perivascular and peribronchiolar lymphocytic infiltration and damaged alveoli were detected in PPE-challenged mice. Scale bar: 100 μm. (**F**) Airway obstruction presented by measuring the percentage of airway luminal area containing AB/PAS-stained material in 1 entire lung section per animal; n = 4–9 animals/group, median ± IQR, saline vs. PPE (**P = 0.001), inactivated PPE vs. PPE (*P = 0.01), Kruskal-Wallis test with Dunn's multiple comparisons test. (**G**) Differential white blood cell counts in BALF of vehicle- and PPE-exposed mice; n = 9–17 animals/group, data presented as median ± IQR, neutrophils (***P = 0.0008), eosinophils (****P < 0.0001), macrophages (***P = 0.0005), and lymphocytes (****P < 0.0001), Mann-Whitney U test.

the most abundant proteins in elastase-exposed mice (Figure 5, C and D). These and the other mucus-related proteins found in elastase-induced BALF and mucus plugs were also increased in epithelial cells, but the chitinase-like proteins were relatively more increased in the elastase-induced epithelial cells (Figure 5E). Furthermore, the increased levels of immune response proteins observed in BALF were also found in the epithelial cell fraction (Supplemental Tables 4 and 7). Absolute quantification revealed, in agreement with the BALF, that Muc5ac was only detected after elastase instillation and that Muc5b levels were increased, but — in this case — only 7.6 times (Figure 5F). Muc5b was always more abundant than Muc5ac, with a Muc5ac/Muc5b ratio of 0.3 in mucus plugs, 0.7 in BALF SN, and 0.5 in epithelial cells (Figure 5G).

To support the proteomic results and analyze the tissue localization of key proteins, immunostaining was performed (Supplemental Figure 7 and Supplemental Figure 8). After elastase instillation, Muc5b, Muc5ac, Clca1, and Fcgbp were all found increased in epithelial cells of both bronchi and bronchioles, and they were accumulated in mucus plugs obstructing the airways. The few Muc5ac-positive epithelial cells detected at basal conditions also expressed Muc5b, and after elastase, a higher proportion of cells coexpressed Muc5ac and Muc5b (Supplemental Figure 7E).

Airway mucus in elastase-exposed mice, COPD, and CF appeared stratified, as in colon. Tissue fixation using methanol-Carnoy (called Carnoy) has been shown to preserve the water-rich mucus structure of the intestine (15). When the elastase-exposed mouse airways were fixed this way and stained by AB/PAS, the mucus had stratified lamellar appearance (Figure 6A). When mucus was stained with antibodies against Muc5b (green) and Muc5ac (red), the 2 mucins appeared to form partly separate layers covering the epithelium (Figure 6B),

Protein UniProt ID	Protein names	Gene names	Plugs	BALF			BALF SN			Epithelial cells		
				Rank		Ratio PPE/Saline	Rank		Ratio PPE/Saline	Rank		Ratio PPE/Saline
				Saline	PPE		Saline	PPE		Saline	PPE	
Q9D7Z6	Clca1	Clca1	1	<LOD	4	-	<LOD	4	-	632	3	171
Q91Z98	Chitinase-3-like protein 4	Chi3l4	2	<LOD	6	-	<LOD	8	-	393	2	196
Q61114	BPI fold-containing family B 1	Bpifb1	3	136	52	6	159	66	6	271	35	8
E9Q5I3	Protein Muc5b	Muc5b	4	<LOD	96	-	<LOD	118	-	547	48	16
E9QAQ8	Protein Muc5ac	Muc5ac	5	<LOD	164	-	<LOD	187	-	< LOD	124	-
Q921I1	Serotransferrin	Tf	6	2	1	2	2	1	2	626	573	1
Q06318	Uteroglobin	Scgb1a1	7	1	2	0.5	1	2	0.4	5	5	1
E9Q9C6	Fcgbp	Fcgbp	8	<LOD	71	-	<LOD	46	-	<LOD	84	-
P60710	Actin, cytoplasmic 1	Actb	9	203	<LOD	-	<LOD	<LOD	-	<LOD	<LOD	-
O35744	Chitinase-3-like protein 3	Chi3l3	10	23	3	13	23	3	15	1265	78	37
P35242	Surfactant-associated protein A	Sftpa1	11	3	14	0.5	10	24	0.7	717	300	3
P08074	Carbonyl reductase [NADPH] 2	Cbr2	12	41	85	0.5	58	89	0.5	1	1	1
Q6ZWY9	Histone H2B type 1-C/E/G	Hist1h2bc	13	53	15	7	153	88	3	4	6	1
Q9EP95	Resistin-like alpha	Retnla	14	230	22	48	<LOD	22	-	1594	42	114
A1L0U3	Histone H3.2	Hist1h3e	15	40	10	5	220	64	13	273	344	1
O09131	Glutathione S-transferase omega-1	Gsto1	16	62	78	1	42	51	1	46	26	2
P01027	Complement C3	C3	17	15	8	2	15	6	3	1305	172	17
P07758	Alpha-1-antitrypsin 1-1	Serpina1a	18	25	29	1	27	21	2	<LOD	<LOD	-
P11276	Fibronectin	Fn1	19	365	12	275	235	10	186	<LOD	1128	-
Q61878	Bone marrow proteoglycan	Prg2	20	<LOD	34	-	<LOD	133	-	<LOD	<LOD	-
P62806	Histone H4	Hist1h4a	21	81	45	3	<LOD	100	-	8	9	1
P27773	Protein disulfide-isomerase A3	Pdia3	22	182	79	6	<LOD	155	-	32	23	1
Q6PAC1	Gelsolin	Gsn	23	152	291	0.3	119	255	0.2	487	438	1
P09103	Protein disulfide-isomerase	P4hb	24	250	124	5	314	183	4	49	37	1
P20152	Vimentin	Vim	25	34	44	1	311	134	8	<LOD	<LOD	-

Figure 3. Most abundant proteins (excluding albumin) detected by mass spectrometry in airway mucus plugs obtained from mice exposed to PPE and changes induced in the epithelial cell and BALF proteome in vivo. BALF, bronchoalveolar lavage fluid; ID, identification; LOD, limit of detection; SN, supernatant. Color code: red (most abundant) to yellow (least abundant) as found in the plugs.

resembling the inner mucus layer of the normal mouse distal colon (Figure 6C). Similar stratified mucus was also observed in lungs from human COPD (Figure 6D) and CF patients obtained at lung transplantation (Figure 6E). Lung tissue from control individuals and COPD and CF patients was stained for MUC5B and MUC5AC, showing a mucus layer that stained for both mucins in the COPD and CF sections (Figure 6, F–H). A stratified mucus appearance was not observed in control lungs. Thus, the mucus accumulated in the elastase model resembled that of COPD and CF chronic lung diseases, with an appearance similar to that of the stratified inner colonic mucus.

Airway mucus in elastase-exposed mice separates bacteria from the epithelial surface. To further illustrate the surface mucus and if it showed evidence for being attached to the tracheobronchial surface, we stained Carnoy-fixed tissue sections taken after 2 PBS washings of 20 minutes with antibodies against Muc5ac and Muc5b, and we analyzed this by confocal microscopy (Figure 7A). The epithelial cell surface was covered by a mucus layer containing a mixture of the Muc5ac and Muc5b mucins. Both mucins were retained and anchored in every goblet cell. As it has been proposed that the stagnated lung mucus is attached by entangling into the cilia (16), we also stained tissue sections for cilia using an anti-tubulin antibody (Figure 7B). The image shows how the cilia extended between the Muc5b-stained mucus, and it does not support that the cilia were entangled with the mucus. In control mice, no clear mucus layer stained by Muc5b was observed (Supplemental Figure 9A).

To understand the importance of the accumulated mucus, we first exposed mice to elastase and then instilled their lungs with *Pseudomonas aeruginosa*, fixed the tissue with Carnoy, and analyzed tissue sections after immunostaining the mucus and *Pseudomonas*. The bacteria were found on the mucus stained by Muc5ac and also inside the mucus, but it was rarely close to the epithelial cells in the bronchi (Figure 7C). In saline-treated mice, no mucus was observed, and the bacteria were in contact with the epithelial cells (Figure 7D). To further illustrate that bacteria were trapped in the attached mucus, *Pseudomonas* were instilled in the lungs, followed by 2 BAL washings with saline or 7% sodium chloride (Supplemental Figure 9, B and C). The bacteria were still found trapped in the mucus. Together, these results suggest that mucus covering the tracheobronchial tree trapped bacteria and separated them from the epithelium, just as has been observed for the inner colon mucus layer.

Mucus is anchored to the goblet cells in elastase-exposed mouse airways and cannot be completely washed away. To analyze if the accumulated mucus was attached to the epithelium in elastase-instilled mouse airways as it has been shown in the CF mouse ileum (15), we lavaged elastase-exposed lungs twice with PBS. The mucus looked less dense after this treatment, as assessed from Carnoy-fixed tissue sections stained with AB/PAS (Figure 8A). Using these sections, we analyzed the percentage of total airways that were obstructed by mucus in nonwashed and in PBS-lavaged lungs. There was a tendency for less airway obstruction in the elastase-exposed mouse airways after PBS lavage (Figure 8B). We also estimated the proportion of the airway surface that was covered by mucus before or after washing. There was essentially no mucus covering the epithelium after saline or inactivated elastase exposure, but after elastase-exposure, there was substantially more airway epithelial surface covered by mucus (Figure 8C). Interestingly, the PBS lavage did not remove any of the mucus on the surface of elastase-exposed airways.

As the accumulated mucus contained both the Muc5b and Muc5ac mucins, we next addressed the importance of these individual mucins using KO animals. The Muc5b$^{-/-}$ mice showed significantly reduced mucus obstruction, whereas the Muc5ac$^{-/-}$ only showed a tendency to reduced mucus obstruction (Figure 8D). The difference between the 2 mucins was even more pronounced when the mucus coverage was analyzed, as the Muc5b$^{-/-}$ showed considerably less mucus coverage (Figure 8E), arguing for the Muc5b mucin being the most important for the mucus accumulation.

We have previously shown that hypertonic saline treatment, approved for use in treatment of CF pulmonary disease, can detach the abnormally attached mucus of the CF mouse ileum. To evaluate if hypertonic saline could remove the attached mucus in the elastase-exposed lungs, we instilled 7% hypertonic saline twice into the lungs, left it for 20 minutes each time, and aspirated the remaining liquid. As a control,

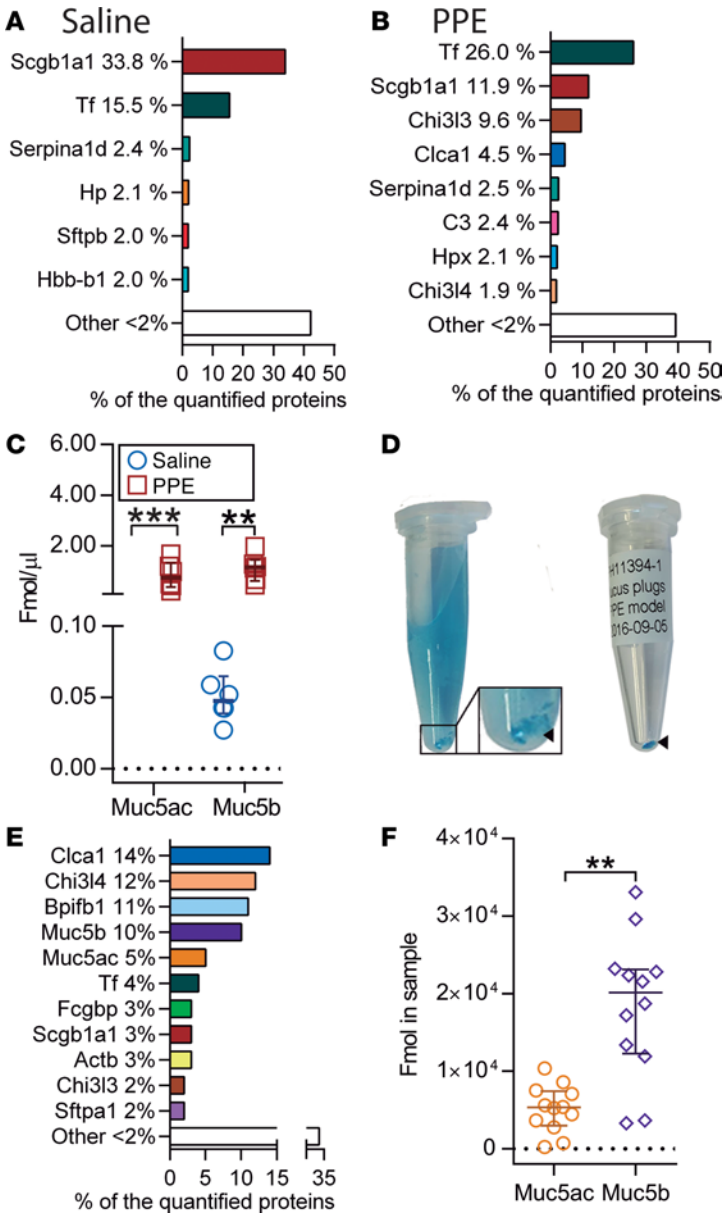

Figure 4. Elastase (PPE) administration alters BALF proteome. (**A** and **B**) Major proteins in BALF supernatants obtained from lungs lavaged with PBS in animals exposed to saline (**A**) and elastase (PPE) (**B**) analyzed by mass spectrometry proteomics. (**C**) Absolute amounts of Muc5ac and Muc5b in BALF supernatant from saline- and PPE-exposed mice analyzed by mass spectrometry. The detection limit for Muc5ac was set to 0.01 fmol/µl, n = 6 animals/group in **A–C**; data presented as median ± IQR, $^{**}P$ = 0.002, $^{***}P$ = 0.0002; Mann-Whitney U test. (**D**) Isolation of mucus plugs from BALF in a PPE-exposed mouse after lavage with an Alcian blue solution. Blue-stained mucus plugs (arrowhead) were obtained and transferred to a dry tube (right). (**E**) The most abundant proteins in mucus plugs detected by proteomics. (**F**) Absolute quantification of Muc5ac and Muc5b protein amounts in mucus plugs by mass spectrometry; data presented as median ± IQR, n = 12 animals in **E** and **F**, $^{**}P$ = 0.0011, Mann-Whitney U test.

we instilled PBS twice for 20 minutes. The hypertonic saline treatment caused a significant decrease in the percentage of airways that were obstructed by mucus (Figure 8F). When the airway surface covered by mucus was evaluated, there was almost no reduction (Figure 8G). Thus, the 7% hypertonic saline could remove most of the mucus plugging, but the surface-attached mucus remained.

To characterize the properties of the accumulated mucus, tracheobronchial explants were stained by AB and the mucus movement was analyzed on an upwardly tilted setup (7). The movement of the AB-stained mucus was considerably slower in the elastase-exposed animals (Figure 8H). Together, these results suggest that the accumulated mucus in the elastase-exposed mouse airways is attached to the goblet cells and is relatively immobile, consistent with the results previously found for the CF mouse small intestine (17).

Discussion

Airway diseases such as COPD and CF involve impaired mucociliary clearance, which leads to mucus accumulation, bacterial retention, bacterial colonization, tissue destruction, and eventually respiratory failure. The mechanisms behind mucus retention and plugging of the airways are, despite considerable efforts, largely unknown. The use of human bronchial epithelial (HBE) cultures has provided important information on the mucus properties of obstructive lung diseases such as CF or COPD, but the relevance

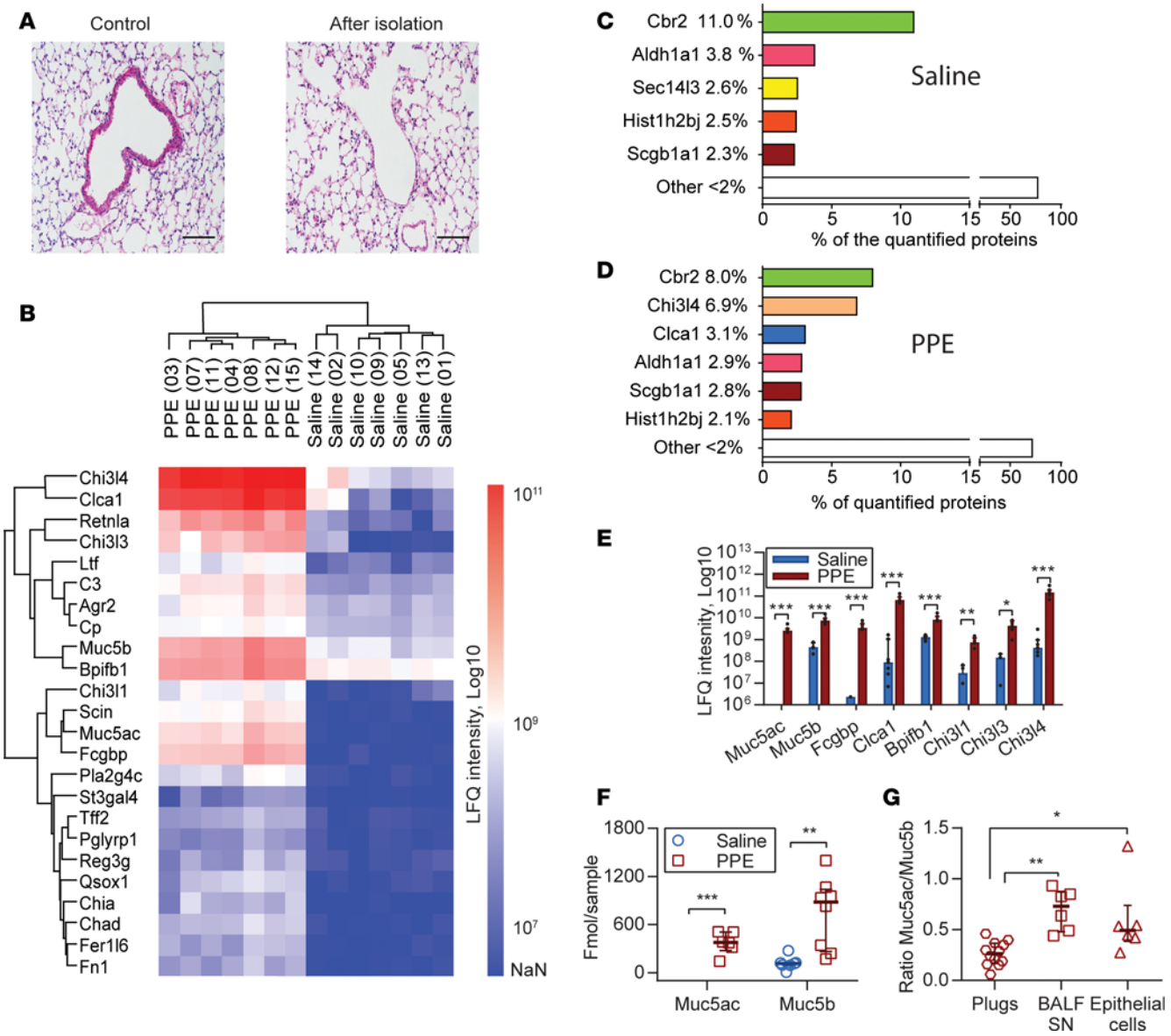

Figure 5. Airway epithelial cell proteome changes after elastase (PPE) administration. (**A**) H&E-stained section of bronchi before (left) and after epithelial cell isolation (right). Scale bars: (left) 200 μm, (right) 50 μm. (**B**) Heatmap of the most changed proteins in the airway epithelial cell proteome after PPE exposure. (**C** and **D**) The most abundant proteins in airway epithelial cells detected by label-free proteomics after saline (**C**) and PPE (**D**) instillation. (**E**) Label-free quantification (LFQ) of the most changed proteins after PPE exposure, n = 7 pools/group with 3 mice/pool, data presented as median ± IQR, $^*P$ = 0.017, $^{**}P$ = 0.006, $^{***}P$ = 0.0006, Mann-Whitney U test. The detection limit for Muc5ac was set to 1×10^6. (**F**) Absolute quantification of Muc5ac and Muc5b with isotopically labeled peptides by mass spectrometry; n = 8 pools/group with 3 mice/pool, data presented as median ± IQR, $^{**}P$ = 0.001, Mann-Whitney U test. Detection limit for Muc5ac was set to 1 fmol. (**G**) Ratio of Muc5ac to Muc5b in isolated mucus plugs, BALF supernatants (BALF SN), and epithelial cells, n = 6–12 samples/group. Data presented as median ± IQR, $^*P$ = 0.04, $^{**}P$ = 0.0016, Kruskal-Wallis and Dunn's multiple comparisons test. Chi3l4, chitinase-3-like protein 4; Clca1, chloride channel accessory 1; Retnla, resistin-like α; Chi3l3, chitinase-3-like protein 3; Ltf, lactotransferrin; C3, complement C3; Agr2, anterior gradient protein 2 homolog; Cp, ceruloplasmin; Bpifb1, BPI fold-containing family B member 1; Chi3l1, chitinase-3-like protein 1; Scin, adseverin; Fcgbp, Fcgbp protein; Pla2g4c, Pla2g4c protein; St3gal4, β-galactoside α-2,3-sialyltransferase 4; Tff2, trefoil factor 2; Pglyrp1, peptidoglycan recognition protein 1; Reg3g, regenerating islet-derived protein 3-γ; Qsox1, sulfhydryl oxidase 1; Chia, acidic mammalian chitinase; Chad, chondroadherin; Fer1l6, Fer-1-like 6; Fn1, fibronectin; Cbr2, carbonyl reductase [NADPH] 2; Aldh1a1, retinal dehydrogenase 1; Sec14l3, SEC14-like 3; Hist1h2bj, histone H2B; Scgb1a1, uteroglobin.

of this model for lung diseases is not fully understood (16). With the aim to utilize a convenient animal model for goblet cell hyperplasia and mucus retention, we chose i.n. instillation of elastase in mice. An increased number of neutrophils and their release of elastase is considered a hallmark in the development of COPD (18). We instilled PPE twice with an interval of 7 days before analyzing the animals after 7 additional days. We studied the elastase-exposed mice by histological examination, analysis of immune cells

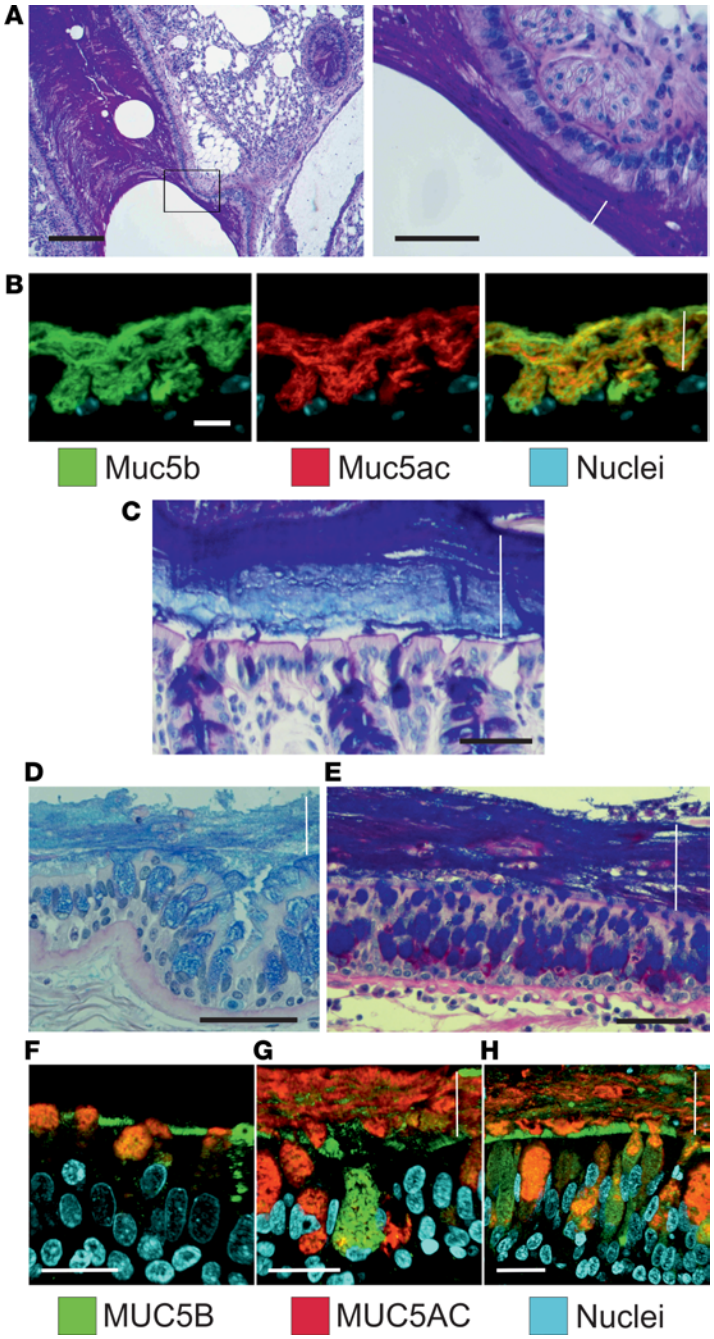

Figure 6. Airway mucus accumulated after elastase administration in mice has a stratified appearance. (**A**) Lower (left) and higher magnification (right) images of an AB/PAS-stained paraffin section showing bronchial walls lined by mucus with lamellar appearance in a mouse exposed to PPE. Representative of 9 animals. Scale bars: left, 200 μm; right, 50 μm. In this and the other pictures, the white line marks the mucus layer. (**B**) A paraffin section from a mouse exposed to PPE stained with specific antibodies against Muc5b (green) and Muc5ac (red), in addition to nuclear stain (blue), shows that this stratified structure consisted Muc5b and Muc5ac. Representative of 3 animals. Scale bar: 10 μm. (**C**) The stratified appearance of mucus has been observed in the distal colon, where the mucus is organized to separate the epithelium from bacterial contact in humans as well as mice. Representative image showing mouse distal colon in an AB/PAS-stained paraffin section. Scale bar: 50 μm. In airway sections from patients with (**D**) COPD and (**E**) cystic fibrosis stained with AB/PAS, stratified mucus can be observed covering the epithelium. Scale bars: 50 μm. In mice as well as humans, mucus does not accumulate in the airways in (**F**) control subjects. Section from patients with (**G**) COPD and (**H**) cystic fibrosis stained with antibodies against MUC5B (green) and MUC5AC (red), in addition to nuclear stain (blue), shows a stratified structure of MUC5B and MUC5AC in the mucus. The MUC5B cell surface staining in **F** could be due to cross-reactivity. Scale bars: 20 μm.

and inflammatory mediators, and proteomics of BALF and epithelial cells. The elastase exposure activated pathways, resulting in a dramatic goblet cell hyperplasia and metaplasia. The mouse lungs showed mucus accumulation with a patchy profile characteristic for human chronic bronchitis and COPD. Severe mucus obstruction was observed, especially in medium-sized airways.

Increased inflammation is characteristic of the airway diseases chronic bronchitis, COPD, CF, and asthma. The inflammatory response in elastase-exposed mice was dominated by eosinophils, but neutrophils, macrophages/monocytes, and lymphocytes were also increased. The mouse lungs are different from those of humans, as they have few submucosal glands; therefore, the elastase mouse model cannot be an exact model for any particular human disease, but it has traits of chronic bronchitis, CF, and possibly also late and severe asthma. For example, among the chemokines upregulated in elastase-exposed mice, we found KC, a murine homologue of IL-8. Higher concentrations of IL-8 have been detected in sputum from COPD patients than in asthmatics, and IL-8 has been correlated with poor lung function in COPD (19).

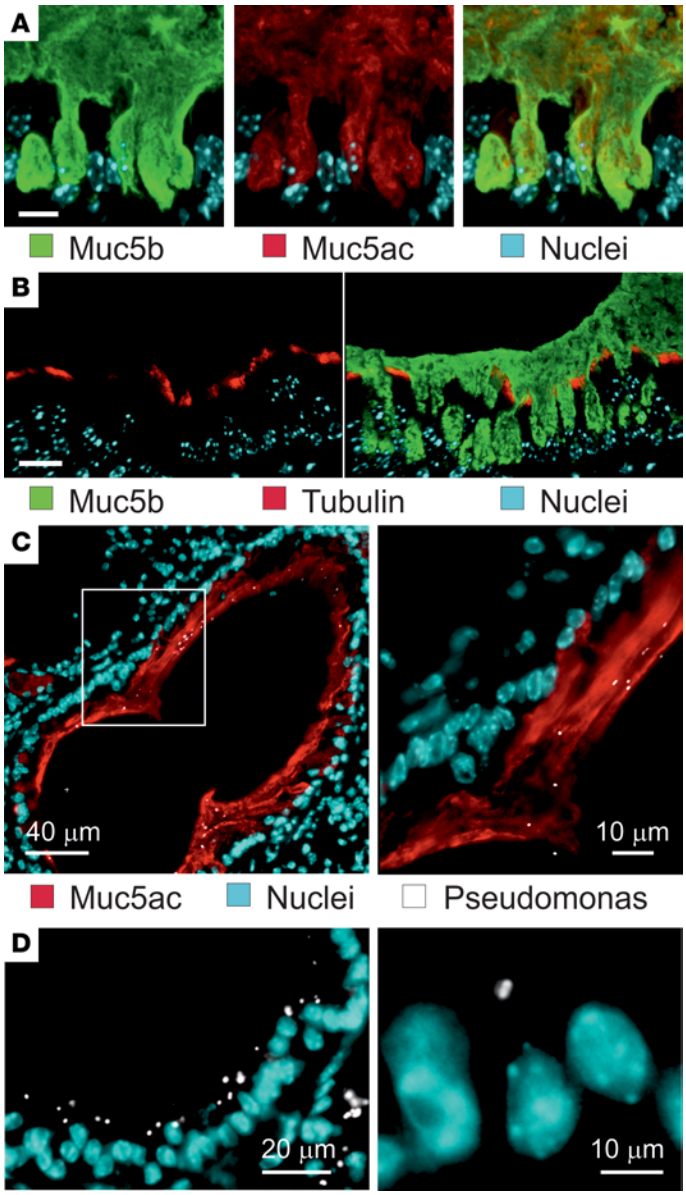

Figure 7. Accumulated airway elastase–exposed mucus is anchored in the goblet cells and separate bacteria from the epithelial cells. (**A**) Immunostaining of a paraffin section with specific antibodies against Muc5b (green) and Muc5ac (red), in addition to nuclear stain (blue). Both Muc5b and Muc5ac seem to be attached inside goblet cells. Representative of 4 mice. Scale bar: 20 μm. (**B**) Immunostaining of a paraffin section from a PPE-exposed mouse with specific antibodies against Muc5b (green) and tubulin (red) to visualize cilia, in addition to nuclear stain (blue). The cilia are not compressed by the accumulated mucus. Representative of 3 mice. Scale bar: 20 μm. (**C**) PPE-exposed mice were instilled with *P. aeruginosa*, and the lungs isolated, fixed in Carnoy, and immunostained for Muc5ac (red), bacteria (white), and nuclei (blue). (**D**) *P. aeruginosa* were instilled in saline-treated mice (control) and stained as in **C**. Representative of 6 PPE-exposed and 3 saline-exposed mice.

In asthma, but also in some patients with COPD, the lung mucosa is infiltrated by eosinophils, and Th2 cells contribute to tissue damage. The Th2 cells produce cytokines, such as IL-4, IL-5, and IL-13 (20) — of which, IL-4 and IL-5 were also increased in the elastase-induced model. Thus, the elastase model showed immunological characteristics that are relevant for studying mucus accumulation in airway diseases.

We have previously performed extensive MS proteomic studies of the mouse gastrointestinal mucus (21, 22). In normal mouse colon mucus, Clca1, Fcgbp, Agr2, and Zg16 are among the most abundant proteins, similar in amount to the main intestinal gel-forming mucin, Muc2. All of these proteins are made by the colonic goblet cells. The proteome of BALF, mucus plugs, and epithelial cells from the lungs of elastase-exposed mice showed increased levels of all these proteins as compared with controls, except for Zg16, which is not present in mouse lungs. Normal mouse lungs rarely express the gel-forming Muc5ac mucin, but this was dramatically induced together with Muc5b after elastase exposure, and other proteins — like Bpifb1, Chi3l1, Chi3l3, and Chi3l4 — were highly increased after elastase exposure. Bpifb1, also called Lplunc1, has been shown to be increased in sputum of COPD, as well as in CF patients, compared with nonsmokers (23, 24).

Proteomic studies on human BALF from COPD patients were performed to evaluate the similarities with the BALF of elastase-exposed mice. Interestingly, PCA clearly distinguished never-smokers, asymptomatic smokers, and COPD patients. The never-smokers and the asymptomatic smokers clustered

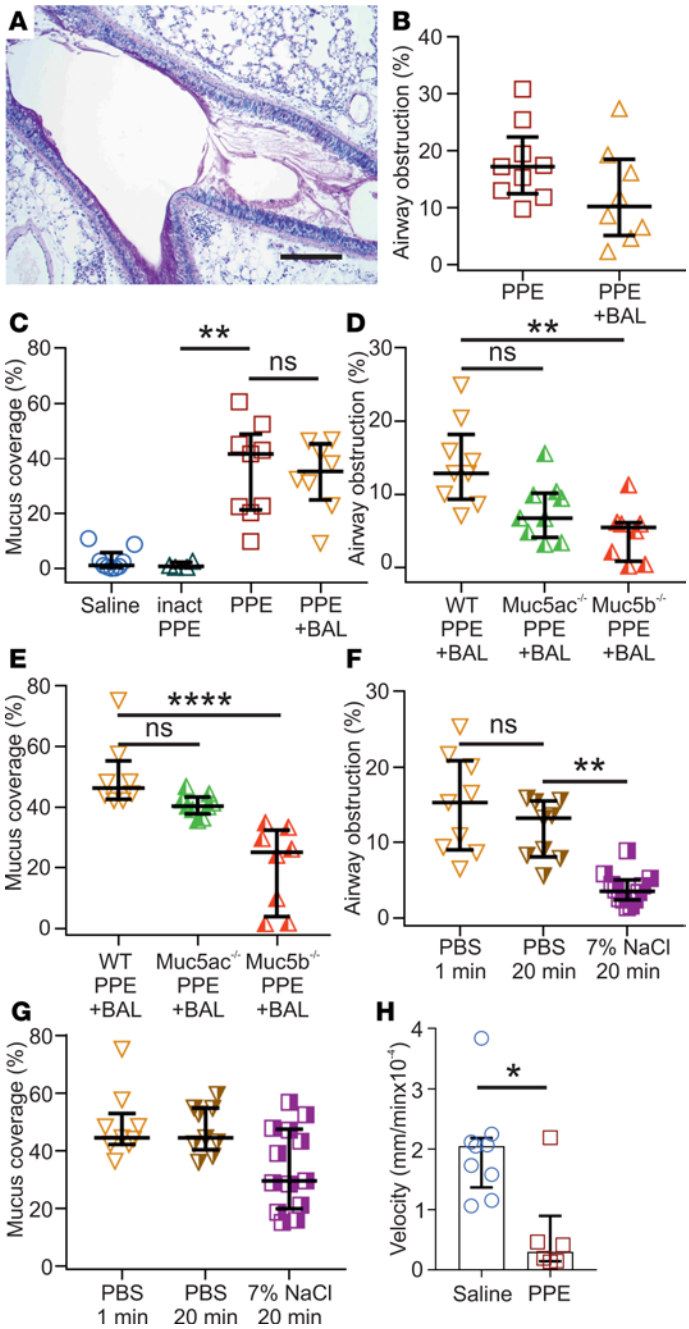

Figure 8. Accumulated airway elastase (PPE) mucus is attached to the epithelium and can be removed by hypertonic saline. (**A**) Representative image of an airway from a mouse exposed to PPE and lavaged with PBS (BAL; 2 × 1 min). Paraffin section stained with AB/PAS. Representative of 8 animals. Scale bar:200 μm. Note the lighter AB/PAS staining and the mucus still covering the epithelial surface. (**B**) Percentage of airway obstruction measured as airway luminal area containing AB/PAS-stained material in an entire lung section per animal. *n* = 8–9 animals/group, 695–729 airway sections/group. BAL was performed by washing 2 × 1 min with PBS. Results presented as median ± IQR. (**C**) Graph showing the large increase in percentage of airway surface covered by AB/PAS-stained material in mice exposed to PPE compared with inactivated PPE. The inactivated PPE gives no increase in surface area covered by mucus, corroborating that the enzymatic activity of PPE-induces the mucus accumulation. In addition, two 1-min washes with PBS did not affect the percentage of epithelium covered by mucus after PPE exposure; *n* = 4–9 animals/group, median ± IQR, $^{**}P = 0.009$, Kruskal-Wallis and Dunn's multiple comparisons test. (**D**) Airway obstruction after BAL (2 × 1 minute) in PPE-treated Muc5ac$^{-/-}$ and Muc5b$^{-/-}$ as compared with WT, *n* = 8-9, $^{**}P = 0.011$, Kruskal-Wallis and Dunn's multiple comparisons test. (**E**) Percentage of airway surface covered by AB/PAS-stained material after BAL (2 × 1 minute) in PPE-exposed Muc5ac$^{-/-}$ and Muc5b$^{-/-}$ mice as compared with WT; *n* = 8–9, $^{****}P < 0.0001$, Kruskal-Wallis and Dunn's multiple comparisons test. (**F**) Airway obstruction was reduced after 2 × 20 min treatment with 7% saline, compared with 2 × 20 min wash with PBS measured in AB/PAS-stained paraffin sections; *n* = 9–12 animals, $^{**}P = 0.002$, Kruskal-Wallis and Dunn's multiple comparisons test. (**G**) The percent of the epithelium covered by mucus was not affected by 2 × 20 min 7% saline treatment measured in AB/PAS-stained paraffin sections; *n* = 9–13 animals, Kruskal-Wallis and Dunn's multiple comparisons test. (**H**) Transport of Alcian blue–stained mucus in naive and PPE-exposed mice; *n* = 6–9, $^{*}P = 0.02$, Mann-Whitney *U* test.

well together, while the COPD patients were spread, revealing a large heterogeneity. Comparison of the absolute amounts of selected proteins, known to be associated with mucus, showed that all were increased in COPD patients regarding never-smokers, with the values in asymptomatic smokers between them. In accordance with the elastase-exposed mice, the 2 mucins (MUC5AC and MUC5B), AGR2, and FCGBP were all increased in COPD. The AGR2 has been suggested to be involved in mucin assembly, although its function is not yet fully understood (25, 26). The FCGBP protein has von Willebrand D domains similar to the ones in the gel-forming mucins, but the function of FCGBP is still an open question. Another known goblet cell product, trefoil factor 3 (TFF3), was found in the normal human intestine and COPD airways (27, 28). DMBT1, a scaffolding protein involved in binding bacteria facilitating their removal, was also increased in BALF from COPD (29). The prostate stem cell antigen (PSCA) was increased in COPD patients compared with asymptomatic smokers and never-smokers. Interestingly, PSCA has been suggested to act as a negative regulator of the α7 nicotinic receptors and to inhibit nicotine signaling (30), something that might be related to nicotine intake, as all COPD patients were smokers. Increased amounts of

transglutaminase 2 (TGM2), which forms isopeptide bonds between the side chains of the amino acids lysine and glutamine, have previously been observed in COPD (31), indicating that lung mucins also can be covalently crosslinked as observed in colon (32).

Comparison of the lung BALF proteome between humans and mice revealed some discrepancies, probably related to the differences between species. The chitinase-like proteins were more abundant in mice. Nonetheless, the CHI3L1 found in airway epithelial cells is a marker of human asthma severity and declining lung function (33). The Clca1 protein, a typical colon mucus protein, was dramatically increased in the elastase-exposed mice but not in human BALF. Clca1 was first suggested to be related to chloride ion channels, but more recent studies have shown that it is a protease that might be involved in mucus turnover (34). The ZG16 protein produced by goblet cells is abundant in mouse and human colonic mucus where it protects the epithelial cells by aggregating gram-positive bacteria, translocating them away from the epithelial cell surface (35). This protein is absent in the human BALF, but a similar protein named ZG16B was dramatically increased in COPD patients. However, this protein was not present in mice.

Increased levels of the 2 gel-forming mucins, MUC5AC and MUC5B, are probably the most typical alteration in the human lung diseases chronic bronchitis, COPD, and CF, as well as in animal models of these diseases (36). This was corroborated in both the elastase mouse model and the human COPD samples studied here. This common feature is irrespective of the different organization of the normal mucus-producing cells in mice and humans, where the latter have submucosal glands that make long MUC5B bundles (7). In normal mice, the surface goblet cells produce mostly the Muc5b mucin, but there is a dramatic increase in the Muc5ac produced upon the induction of goblet cell hyperplasia. The MUC5B mucin forms linear polymers responsible for normal clearing of the lungs in both species (37), whereas MUC5AC, with its more complex polymers, is typical for normal pig and human surface goblet cells and appears in all 3 species during disease. The ratio between these 2 mucins was similar in BALF from the elastase-exposed mice and COPD patients, suggesting that the composition of the accumulated mucus should be similar despite the large differences in normal lung function of mice and humans. Our results suggest that Muc5b contributed the most to mucus obstruction, given its high levels in both mucus plugs and in BALF washings of elastase-treated Muc5ac-KO mice. This relatively larger importance of Muc5b in mice is also observed for normal lung clearance (8). Even if we do not fully understand the details of how these 2 mucins contribute to mucus properties, it may suggest that the accumulated disease-associated mucus has similar features in the 2 species.

The protein composition of the mucus accumulated in the elastase-exposed mice and COPD shows large similarities to that of the inner mucus layer of colon in both mice and humans. Even more intriguing is that the structure of the accumulated mucus in COPD, CF, and elastase-exposed mice shows a stratified arrangement, closely resembling that of the inner mucus layer of the normal colon (15). In the colon, the inner mucus layer acts as a barrier that physically separates the luminal bacteria from the epithelial surface (15). This separation is obtained by the MUC2 mucin–forming net-like sheets that, when layered on each other, form a filter and thereby protect the epithelial cells. To analyze if this was also the case in the elastase-exposed mice, we exposed the lungs to *P. aeruginosa*. The bacteria were found on the mucus surface, as well as inside the mucus. This is not typically observed for normal colon but can be observed in the mucus covering the stomach (38). Interestingly, as in the lung, the stomach mucus is made up of the Muc5ac mucin. Without a mucus layer, the bacteria were in direct contact with the epithelial cells. It is then reasonable to believe that the tracheobronchial airway mucus layer may act as an innate defense mechanism aimed at trapping and keeping the bacteria away from the host epithelial cell surface. Although it can be assumed that accumulated and adherent mucus will limit bacterial clearance, this has to be experimentally addressed in the presence or absence of the adherent mucus layer and its effect on the epithelial invasion tested.

Washing the elastase-exposed mouse lungs with PBS partly removed the mucus plugs blocking the more peripheral airways. However, a similar proportion of the epithelial surface was covered by mucus before or after washing, suggesting that the mucus was attached to the surface. Studies of tissue sections, also after intense washings, suggested that the mucus and, in particular, the 2 mucins were anchored to the goblet cells. Interestingly, this is similar to what has been observed for mucus in the CF small intestine, where the Muc2 mucin is not properly unfolded and, thus, not released from its attachment by the meprin β protease (17, 39). To test if the commonly used CF treatment, hypertonic saline, could detach the mucus, we treated the elastase-exposed mice 2 times with 7% NaCl. Hypertonic saline significantly decreased airway mucus obstruction more efficiently than PBS. However, this treatment was not better than PBS in

removing the attached mucus covering the epithelial surface. A recent publication has also suggested that the MUC5AC mucin is tethered to the goblet cells in asthma patients (40). Together, these observations suggest that the accumulated mucus is attached to the goblet cells and that this is the main mechanism for obtaining an airway mucus layer.

The normal lung is kept relatively free of bacteria by the cilia-mediated mucus escalator. We suggest that when this mechanism fails, a second line of defense is triggered by the formation of an attached mucus layer, similar to the normal protection of the colon epithelium. The physiological function of this airway mucus layer might, thus, be to separate the epithelial cells from bacterial exposure. This attached stratified mucus layer may be a normal physiological mechanism attempting to separate the bacteria from the epithelial cells to give the immune system a possibility to raise an immune response. Once the bacteria are under control, the mucus should be removed by detachment. However, this type of mucus would not be transported very efficiently by the cilia and probably has to be coughed up, a typical resolution to any lung infection. In chronic lung diseases like chronic bronchitis, COPD, CF, and severe asthma, the mucus probably remains attached, as demonstrated in our experiments, and although the epithelium might be better protected, the bacterial retention would lead to chronic lung infections and lung deterioration. The intriguing question is now the molecular details regulating mucus attachment.

Methods

Animals. Female C57BL/6N (Taconic), Muc5b$^{-/-}$, and Muc5ac$^{-/-}$ (8) mice were used when they were 10 ± 2 weeks old and weighing 21 ± 3 g. Animals were housed in a specific pathogen-free facility in groups of 3 or 4 in controlled temperature (21°C ± 2°C), relative humidity (55% ± 15%) and a 12-hour light/dark cycle. Standard chow and water were available ad libitum.

Elastase administration and BALF collection. Animals under light isoflurane anesthesia were exposed to 0.312 units of PPE (45124, MilliporeSigma), inactivated PPE, or vehicle (50 μl saline) instilled i.n. The instillation procedure was performed at days 0 and 7. Six to 8 days after final exposure, animals were euthanized with an overdose of pentobarbital sodium i.p., and the abdominal aorta was severed. To obtain BALF samples, tracheas were cannulated with a catheter (Venflon, Becton Dickinson). Lungs were manually lavaged twice with 0.8 ml of PBS for 1 minute each, and the 2 lavages were pooled. BALF samples and SNs, obtained after centrifugation (500 *g*, 10 min, 4°C), were stored at –80°C for later analysis. For some of the experiments, the duration of each lavage was increased to 20 minutes, as described in Results. For others, hypertonic saline (7% NaCl) was tested to investigate the ability to detach airway mucus. Chemicals used were provided by Merck.

Blood cell count and inflammatory mediator analysis. Total and differential WBC counts were determined using an automated cell counter (Sysmex XT-2000iV; Sysmex Corporation). Cytokine analysis in BALF SNs was performed using MILLIPLEX MAP Mouse Cytokine/Chemokine Magnetic Bead Panels (MCYTMAG70PMX25BK and MECY2MAG-73K; MilliporeSigma) and the Proinflammatory Panel 1 (mouse) kit (N05048A-1; Meso Scale Discovery). EGF concentrations were determined by ELISA (MEG00; R&D Systems). Assays were performed according to the manufacturer's instructions.

Mucus plug isolation. For mucus plug isolation, BAL was performed with an AB solution in PBS. First, a 5% w/v suspension of Alcian blue 8GX (MilliporeSigma) was prepared in PBS. After mixing overnight (1,000 rpm) in a Thermomixer comfort (Eppendorf) at room temperature, this was centrifuged (14,000 *g*, 10 min, room temperature). The SN was further diluted 1:40 in PBS. Mucus plugs, identified as AB-stained structures in BALF, were transferred with a 10-μl tip to a dry tube, frozen in liquid N_2, and stored at –80°C.

Elastase inactivation. To inactivate the enzymatic activity of PPE, a stock solution of 50 units/ml was incubated with 1 mM PMSF overnight at 4°C. The resulting solution was diluted 1:10 in sterile saline, and 1 ml was loaded in dialysis membrane tubing (Spectrum Spectra/Por 4 RC 12-14 KDa; Thermo Fisher Scientific) and dialyzed against 1 l of saline at 4°C twice (first dialysis, 8 hours; second dialysis, overnight). The inactivated PPE was concentrated using a centrifugal filter (10 kDa pore size; UFC501024; MilliporeSigma). The protein concentration of the inactivated PPE was assessed with a Nanodrop (A280; Thermo Fisher Scientific). The elastase activity of the inactivated PPE, active PPE (positive control), and saline was measured using an EnzChek Protease Assay Kit (Thermo Fisher Scientific). The substrate BODIPY casein was added, and fluorescence, as a measure of cleavage, was read at λ_{ex} 477 ± 14 nm and λ_{em} 525 ± 30 nm every 5 minutes for 1 hour, where λ_{ex} represents excitation wavelengh and λ_{ex} represents emission wavelengh. The percentage of inhibition was calculated for the last reading.

Histopathological analysis. After obtaining the BALF, the thoracic cavity was opened. Lungs used to characterize inflammatory response and goblet cell hyperplasia were perfused through the interventricular septum with 10 ml PBS and then inflated to 25 cm H_2O static pressure by intratracheal instillation of Carnoy (60% anhydrous methanol, 30% chloroform, and 10% glacial acetic acid). The trachea was tied and the inflated lungs removed and immersed in fixative. Lungs used to study airway mucus accumulation and plugging were directly immersed in Carnoy, without previous inflation. Lungs were embedded in paraffin, and sections (3 μm) comprising both the left and the right lung lobes were cut at the level of the tracheobronchial tree. Sections were stained with H&E to evaluate inflammation and structural alterations, stained with AB/PAS to assess goblet cell hyperplasia and mucus accumulation, or used for immunostainings.

Quantification of mucus accumulation. Images of mouse lung sections stained with AB/PAS were obtained at 100× magnification using a Nikon eclipse E1000 microscope and the NIS-Elements software (Nikon). Images of all airway sections included in an entire lung section were captured. ImageJ (NIH) was used for image analysis. The percentage of the lumen area positively stained with AB/PAS for each airway section was measured. For each mouse, we calculated the total percentage of lumen airway obstruction (AB/PAS-positive). In addition, we evaluated for each airway section the minimum Feret's diameter (XFmin), a very robust size measure against experimental errors such as the orientation of the sectioning angle (14). The correlation of XFmin with the percentage of obstruction was assessed in PPE-exposed mice, and the percentage of airway epithelial surface covered by AB/PAS-positive material was calculated.

Immunostainings. Lung tissue sections were dewaxed and rehydrated, and microwave-assisted antigen retrieval was performed in 10 mM citrate buffer, pH 6. Samples were blocked for 20 minutes at room temperature with 5% inactivated goat or donkey serum, according to the species in which the secondary antibodies were produced. Thereafter, sections were incubated overnight at 4°C with a mouse anti-Muc5ac antibody (clone 45M1; M5293, MilliporeSigma; 1:1,000), a rabbit anti-Muc5b/MUC5B antibody (Mehmed Kesimer, University of North Carolina, Chapell Hill, North Carolina, USA1:2,000), a rabbit anti-Clca1 antibody (ab46512, Abcam; 1:1,000), a rabbit anti-Fcgbp antibody (HPA003517, Atlas Antibodies; 1:100), or a mouse monoclonal anti-tubulin antibody (T6793, MilliporeSigma; 1:4,000). In the case of single stains, slides were then incubated for 2 hours at room temperature with goat anti–mouse IgG or donkey anti–rabbit IgG secondary antibodies conjugated to Alexa Fluor 488 or 555 (Thermo Fisher Scientific; A11029 and A31572, respectively; 1:1,000). For colocalization studies, slides were washed, blocked, incubated with a second primary antibody using the same conditions described above, and then incubated for 2 hours at room temperature with the corresponding fluorescently conjugated antibodies (1:1,000). Nuclei were counterstained for 10 minutes using 1 μg/ml Hoechst 34580 (H21486, Thermo Fisher Scientific) and mounted with Prolong Gold Antifade mounting medium (P36930, Thermo Fisher Scientific). The specificity of the primary antibodies used for Muc5ac and Muc5b detection had been previously confirmed by others (41, 42). Concerning the antibodies for Clca1 and Fcgbp, we confirmed that none of them stained sections of colon or PPE-exposed lungs in corresponding KO mice. Nonspecific binding of the secondary antibody was ruled out by omitting the primary antibody. Whole lung sections were scanned using an Axio Scan.Z1 scanner with a 20× Plan-Apochromat 0.8 NA dry objective and ZEN 2.1 software (Carl Zeiss). High-magnification images were obtained using a LSM700 Axio Examiner Z1 confocal microscope with the ZEN 2010 software (Carl Zeiss). Fluorescence intensity per μm^2 was measured with ImageJ and expressed as the relative change compared with the median intensity in saline-treated controls. Analysis of all data was performed in a blinded manner.

P. aeruginosa instillation and localization. *P. aeruginosa* CCUG 44340 (isolated from sputum of a 15-year-old child with CF) were cultured in LB broth overnight at 37°C and at 170 rpm. The bacteria were recovered by centrifugation, resuspended in PBS, and diluted to an optical density at 600 nm (OD600) of 0.98 corresponding to 2×10^8 CFU/ml. PPE-exposed mice were euthanized 1 week after the final dose. *P. aeruginosa* was administered by instilling 200 μl of the culture into the cannulated tracheas. Lungs were isolated, fixed in Carnoy solution, embedded in paraffin, and then sectioned for immunostaining. Paraffin-embedded sections (5 μm) were dewaxed and hydrated. Muc5ac was stained using mouse anti-Muc5ac antibody (clone 45M1; M5293, MilliporeSigma; 1:1,000). Alexa Fluor 488–conjugated goat anti–mouse IgG (Thermo Fisher Scientific) was used as a secondary antibody. *P. aeruginosa* was detected using polyclonal rabbit anti–*P. aeruginosa* antibody (Abcam, Ab68538). Alexa Fluor 555-conjugated donkey anti-rabbit IgG (Thermo Fisher Scientific; A31572) was used as secondary antibody. Sections were counterstained using Hoechst 33258 (MilliporeSigma). Stained sections were mounted in Prolong Anti-fade (Invitrogen).

Images of stained mouse lung sections were obtained at 40× and 100× magnification using a Nikon eclipse E1000 microscope and the NIS-Elements software (Nikon).

Transmission electron microscopy. Mouse lungs were fixed in modified Karnovsky's fixative (2% paraformaldehyde, 2.5% glutaraldehyde in 0.05 M, sodium cacodylate buffer, pH 7.2) for 24 hours. One lung lobe was divided into 9 transverse sections, and every other section starting from the second section was processed further for electron microscopy. Samples were sequentially stained using 1% OsO_4 for 4 hours, 1% tannic acid for 3 hours, and 1% uranyl acetate overnight; they were then dehydrated and embedded in epoxy resin (Agar 100, Agar Scientific). Electron microscopy was conducted on 50-nm sections cut using an Ultracut E (Reichert) microtome and collected on mesh copper support grids. Contrast was added to the sections using lead citrate and tannic acid, and images were acquired using a LEO 912 transmission electron microscope (Carl Zeiss) operated at an accelerating voltage of 120 kV.

Isolation of epithelial cells. After obtaining BALF, lungs were washed twice through the intratracheal cannula with 0.8 ml PBS, and the liquid was discarded. Thereafter, epithelial cells were isolated using a predisgestion buffer (20 mM EDTA and 1 mM DTT in HBSS without Ca^{2+} or Mg^{2+} supplemented with 10 mM HEPES). Initially, 0.8 ml of prewarmed predigestion buffer was instilled through the intratracheal cannula. Lungs were immersed in prewarmed PBS and placed in a water bath at 37°C, where they remained during the whole procedure. Lungs were then washed with 0.8 ml of prewarmed predigestion buffer once at 15. 30, and 45 minutes and 1 hour after the first instillation. After each lavage, the buffer aspirated from the lungs containing epithelial cells in suspension was transferred to a tube kept on ice. All the lavages obtained from 3 animals belonging to the same group were pooled to obtain each epithelial cell sample. The cell suspension was vortexed for 2 minutes and centrifuged (500 *g*, 10 min, 4°C). The SN was discarded and the cell pellet resuspended in 2 ml HBSS and kept on ice. Erythrocytes were lysed using the ACK Lysing Buffer (Gibco, Thermo Fisher Scientific). Afterward, cell pellets were incubated in 1 ml of collagenase type I (2 mg/ml; 17100-017, Invitrogen) and DNAse I (40 U/ml; D-4513, MilliporeSigma) in DMEM/F12 with HEPES for 30 minutes at 37°C. After enzymatic digestion, cells were washed with 10 ml HBSS, centrifuged (500 *g*, 10 min, 4°C), and resuspended in 2 ml HBSS. The cell suspension was passed through a 30-μm mesh (Miltenyi Biotec) to obtain a single-cell suspension. A sequential negative selection of epithelial cells was performed using MACS separation reagents and instruments (Miltenyi Biotec). Samples were first depleted of CD45-positive cells and then of Ly6G-positive cells, using 2 different MACS LD Depletion columns, microbeads, and MidiMACS magnets (all from Miltenyi Biotec). The procedure was performed according to the manufacturer's instructions, with the exception that columns were washed 3 times instead of 2, to maximize the recovery of unlabeled cells, and that the incubation with Anti–Ly-6G-Biotin beads was increased from 10 to 30 minutes, to improve neutrophil depletion. At the end of the procedure, the magnetically unlabeled cell fraction containing epithelial cells was collected. Ice-cold PBS was added to a total volume of 14 ml, samples were centrifuged (500 *g*, 10 min, 4°C), and the SN was discarded. Cells were resuspended in 1 ml PBS, transferred to MCT-175-L-C tubes (Axygen), and centrifuged (1,000 *g*, 5 min, 4°C). After the SN was completely removed, pellets were frozen in liquid N_2 and stored at –80°C.

Presence of leukocytes and neutrophils in the airway epithelial cell suspension was detected by flow cytometry. Cell suspensions from the different fractions, $CD45^+$ (leukocytes), $Ly\text{-}6G^+$ (neutrophils), and $CD45^-Ly\text{-}6G^-$ were washed in FACS buffer (HBSS without calcium, magnesium, and phenol red [HBSSwo], 2% v/v FCS, 5 mM EDTA) and stained with the viability marker Fixable Viability Dye eFluor 780 (Thermo Fisher Scientific) for 30 minutes, on ice and in the dark. After the viability staining, cells were washed in FACS buffer and labeled with anti–EpCAM FITC (G8.8), anti–CD45 PE (30-F11) and anti–Ly-6G-PerCP eFluor710 (1A8-Ly6g) (all from Thermo Fisher Scientific). After the staining (30 minutes, on ice, in the dark), cells were washed with FACS buffer and analyzed by using the FACS Jazz (Becton Dickinson).

MS. Mice BALF (50 μl) and mucus plug samples were incubated overnight at 37°C in reduction buffer (6 M guanidinium hydrochloride [GuHCl], 0.1 M Tris/ HCl pH 8.5, 5 mM EDTA, 0.1 M DTT; Merck) followed by a modified filter-aided sample preparation (FASP) protocol using 6 M GuHCl (43). Briefly, proteins were alkylated on 10 kDa cut-off filters and subsequently digested for 4 hours with LysC (Wako Chemicals), followed by an overnight trypsin (Promega) digestion. Heavy peptides (JPT Peptide Technologies) for Muc5b and Muc5ac absolute quantification (5 peptides for each protein, 100 fmol each; Supplemental Table 8) were added before trypsin digestion. Epithelial cells for proteomics analysis were prepared according to the FASP protocol (44). Briefly, cells were lysed by boiling in 4% SDS, buffer was exchanged to 8 M urea on 30 kDa cut-off filters, and proteins were alkylated and digested for 4 hours with endopeptidase LysC (Wako

Chemicals), followed by overnight digestion with trypsin (Promega). Human BALF (180 μl) was processed as mouse BALF, but heavy labeled peptides (JPT Peptide Technologies) for 15 human proteins were added (100 fmol each; Supplemental Table 8).

Peptides released from the filter by centrifugation were cleaned with StageTip C18 columns as previously described (45). Nano-Liquid-Chromatography MS (NanoLC-MS/MS) was performed on an EASY-nanoLC system (Thermo Fisher Scientific), connected to a Q-Exactive Hybrid Quadrupole-Orbitrap Mass Spectrometer (Thermo Fisher Scientific) through a nanoelectrospray ion source. Peptides from mucus plugs and BALF samples were separated in an in-house packed C18 reverse-phase column (150 × 0.075 mm inner diameter, C18-AQ 3 μm) by a 60-minute gradient from 5%–40% B (A, 0.1% formic acid; B, 0.1% formic acid/80% acetonitrile 200 nl/min). Peptides from epithelial cell samples were separated with a heated (50°C) C18 reverse-phase EASY-Spray column (500 × 0.050 mm, PepMap RSLC, 2 μm, 100 Å) by a 120-minute gradient from 2%–25% B, followed by 10-minute increase to 40% B. Full mass spectra were acquired from *m/z* 320–1,600, for BALF and plugs, or 400–1,600 *m/z*, for epithelial cell pools, with resolution of 70,000. Up to the 12 most intense peaks (charge state ≥2) were fragmented. Tandem mass spectra were acquired with a resolution of 35,000 and automatic dynamic exclusion for BALF and mucus plugs, with a resolution of 17,500 and dynamic exclusion of 10 seconds for epithelial cells. Human BALF samples were analyzed by acquiring full spectra from *m/z* 350–1,600 with a resolution of 70,000. Up to the 10 most intense peaks were fragmented, and tandem mass spectra were acquired with a resolution of 17,500 and dynamic exclusion of 10 seconds. For absolute quantification, a separate targeted MS method was used where only precursors and fragments of the heavy and corresponding light peptides were scanned with a resolution of 35,000.

Proteomic data analysis. Proteomics data were analyzed with the MaxQuant program (version 1.4.1) (46). Searches were performed against the mouse UniProt protein database (downloaded July 23, 2015) or the human Uniprot protein database (downloaded July 23, 2015) supplemented with an in-house database containing all the human and mouse mucin sequences (http://www.medkem.gu.se/mucinbiology/databases/). Searches were performed with full tryptic specificity, with a maximum of 2 missed cleavages, a precursor tolerance of 20 ppm in the first search followed by 7 ppm for the main search, and 0.5 Da for fragment ions. Carbamidomethylation of cysteine was set as a fixed modification, and methionine oxidation and protein N-terminal acetylation were set as variable modifications. The FDR was set to 1% both at the peptide and protein levels, and the minimum required peptide length was set to 6 amino acids. Proteins were quantified by the MaxQuant label-free quantification (LFQ) algorithm, using a minimum of 2 peptides. Data filtering, data clustering, and PCA were performed with the Perseus software (version 1.5.6.0). The data was filtered based on the presence of a protein group in at least 3 of 6 biological replicates for BALF, 4 of 7 replicates for epithelial cells, and 6 of 12 replicates for plugs. Missing values were replaced from the normal distribution. Albumin was excluded as contaminant. Hierarchical clustering was obtained using the Euclidean distance, with average linkage and preprocessing with k-means for rows and columns. Results were plotted as heatmaps. For PCA, the default parameters were used, obtaining 5 components with the Benjamin-Hochberg method (FDR = 0.05). The MS proteomics data were deposited to the Proteome Xchange Consortium (http://proteomecentral.proteomexchange.org) via the PRIDE partner repository (https://www.ebi.ac.uk/pride/archive/) with the dataset identifier PXD006770. Absolute quantification of proteins that had heavy-labeled standard peptides (Supplemental Table 8) was performed with the Skyline program (version 3.6.0.1) (47). The median peptide concentration was reported as protein concentration.

Mouse mucus transport in live tissues. Animals were euthanized with an overdose of pentobarbital sodium i.p., and the abdominal aorta was severed. Both trachea and the connected lungs were isolated. The trachea and proximal part of the primary bronchi were opened and mounted in a Petri dish coated with Sylgard 184 Silicone Elastomer (Dow Corning) using 27 G needles. The tissue was covered in 0.4 mM Alcian blue 8GX diluted in oxygenated (95% O_2, 5% CO_2) Krebs-glucose buffer in 116 mM NaCl, 1.3 mM $CaCl_2$, 3.6 mM KCl, 1.4 mM KH_2PO_4, 23 mM $NaHCO_3$, and 1.2 mM $MgSO_4$, 10 mM d-glucose, 5.7 mM pyruvate, and 5.1 mM glutamate, pH 7.4, and gradually heated to 37°C. The tissue was monitored through a stereo microscope. The mean speed of the moving AB-stained mucus in each time-lapse was calculated using NIS-Elements (Nikon) (mean of 2–5 measurements). Then, the mean of the speed of 2–6 time-lapses/mouse was calculated.

Patient samples. BALF samples were collected from healthy never-smokers, healthy smokers, and patients with diagnosed COPD. The clinical characteristics for these patients are summarized in Supplemental Table 5.

Statistics. Results are presented as median ± interquartile range (IQR) or mean ± SEM. For comparision of 2 independent groups, we used the Mann-Whitney *U* test; for comparison of multiple groups, we used the Kruskal-Wallis test, with Dunn's post-hoc test to correct for multiple comparisons. The number of biological replicates is indicated by *n* (number of animals or samples when several animals were pooled to obtain 1 data point). Significance was defined as $P < 0.05$. For statistics on proteomic data analysis, the Benjamin-Hochberg method (FDR 0.05) was used.

Study approval. Care and use of animals was undertaken in compliance with the European Community Directive 2010/63/EU. Animal experiments were approved by the local ethics committee in Gothenburg with the ethical permit numbers 100-2014 and 75-2015. Human samples were acquired with approval by the local human research ethics committee with the permit number 543-11. All human subjects gave written informed consent prior to inclusion, and all investigations were performed in accordance with the Declaration of Helsinki.

Author contributions

JAFB, AE, DF, AÅ, and GCH designed the study. JAFB, DF, LA, AE, AMRP, BMA, ES, and SJ conducted the experiments. SJ, JR, CM, CME, and AÅ provided compounds and materials. DS provided patient samples. JAFB, AE, and GCH wrote the manuscript. All authors approved the manuscript.

Acknowledgments

The work was funded by AstraZeneca, the European Research Council ERC (694181), National Institute of Allergy and Infectious Diseases (U01AI095473; the content is solely the responsibility of the authors and does not necessarily represent the official views of the NIH), The Knut and Alice Wallenberg Foundation, The Swedish Research Council, The Swedish Cancer Foundation, IngaBritt and Arne Lundberg Foundation, Sahlgrenska University Hospital (ALF), Wilhelm and Martina Lundgren's Foundation, The Cystic Fibrosis Foundation (CFF), Swedish CF Foundation, Erica Lederhausen's Foundation, Lederhausen's Center for CF Research at University Gothenburg, Magnus Bergvall's foundation, and the Swedish Heart-Lung Foundation. We thank Mehmed Kesimer (University of North Carolina, Chapell Hill, North Carolina, USA) for the anti-Muc5b antibody. We also acknowledge the Centre for Cellular Imaging at the University of Gothenburg, Lisa Jinton for cytokine analyses, Sofia Lundin for handling of human tissues, and Botilda Lindberg and Susanne Arlbrandt for animal work.

Address correspondence to: Gunnar C. Hansson, Department of Medical Biochemistry, Sahlgrenska Academy, University of Gothenburg, PO Box 440, S-405 30 Gothenburg, Sweden. Phone: 46.31.786.3488; Email: gunnar.hansson@medkem.gu.se.

1. Smaldone GC, Foster WM, O'Riordan TG, Messina MS, Perry RJ, Langenback EG. Regional impairment of mucociliary clearance in chronic obstructive pulmonary disease. *Chest*. 1993;103(5):1390–1396.
2. Regnis JA, et al. Mucociliary clearance in patients with cystic fibrosis and in normal subjects. *Am J Respir Crit Care Med*. 1994;150(1):66–71.
3. Bateman JR, Pavia D, Sheahan NF, Agnew JE, Clarke SW. Impaired tracheobronchial clearance in patients with mild stable asthma. *Thorax*. 1983;38(6):463–467.
4. Vestbo J, et al. Global strategy for the diagnosis, management, and prevention of chronic obstructive pulmonary disease: GOLD executive summary. *Am J Respir Crit Care Med*. 2013;187(4):347–365.
5. Tatsumi K. [Concept of COPD, from past to the present]. *Nippon Rinsho*. 2011;69(10):1713–1720.
6. Ostedgaard LS, et al. Gel-forming mucins form distinct morphologic structures in airways. *Proc Natl Acad Sci USA*. 2017;114(26):6842–6847.
7. Ermund A, et al. The normal trachea is cleaned by MUC5B mucin bundles from the submucosal glands coated with the MUC5AC mucin. *Biochem Biophys Res Commun*. 2017;492(3):331–337.
8. Roy MG, et al. Muc5b is required for airway defence. *Nature*. 2014;505(7483):412–416.
9. Kung TT, et al. Characterization of a murine model of allergic pulmonary inflammation. *Int Arch Allergy Immunol*. 1994;105(1):83–90.
10. Kuperman DA, et al. Direct effects of interleukin-13 on epithelial cells cause airway hyperreactivity and mucus overproduction in asthma. *Nat Med*. 2002;8(8):885–889.
11. Shapiro SD. Animal models for COPD. *Chest*. 2000;117(5 Suppl 1):223S–227S.
12. Gross P, Babyak MA, Tolker E, Kaschak M. Enzymatically produced pulmonary emphysema; a preliminary report. *J Occup Med*. 1964;6:481–484.
13. Conlon TM, et al. Metabolomics screening identifies reduced L-carnitine to be associated with progressive emphysema. *Clin Sci*. 2016;130(4):273–287.

14. Birrer P, et al. Protease-antiprotease imbalance in the lungs of children with cystic fibrosis. *Am J Respir Crit Care Med*. 1994;150(1):207–213.
15. Johansson ME, Phillipson M, Petersson J, Velcich A, Holm L, Hansson GC. The inner of the two Muc2 mucin-dependent mucus layers in colon is devoid of bacteria. *Proc Natl Acad Sci USA*. 2008;105(39):15064–15069.
16. Matsui H, et al. Evidence for periciliary liquid layer depletion, not abnormal ion composition, in the pathogenesis of cystic fibrosis airways disease. *Cell*. 1998;95(7):1005–1015.
17. Gustafsson JK, et al. Bicarbonate and functional CFTR channel are required for proper mucin secretion and link cystic fibrosis with its mucus phenotype. *J Exp Med*. 2012;209(7):1263–1272.
18. Hoenderdos K, Condliffe A. The neutrophil in chronic obstructive pulmonary disease. *Am J Respir Cell Mol Biol*. 2013;48(5):531–539.
19. Yamamoto C, et al. Airway inflammation in COPD assessed by sputum levels of interleukin-8. *Chest*. 1997;112(2):505–510.
20. Lukacs NW. Role of chemokines in the pathogenesis of asthma. *Nat Rev Immunol*. 2001;1(2):108–116.
21. Johansson ME, Thomsson KA, Hansson GC. Proteomic analyses of the two mucus layers of the colon barrier reveal that their main component, the Muc2 mucin, is strongly bound to the Fcgbp protein. *J Proteome Res*. 2009;8(7):3549–3557.
22. Rodríguez-Piñeiro AM, et al. Studies of mucus in mouse stomach, small intestine, and colon. II. Gastrointestinal mucus proteome reveals Muc2 and Muc5ac accompanied by a set of core proteins. *Am J Physiol Gastrointest Liver Physiol*. 2013;305(5):G348–G356.
23. Gao J, et al. Elevated sputum BPIFB1 levels in smokers with chronic obstructive pulmonary disease: a longitudinal study. *Am J Physiol Lung Cell Mol Physiol*. 2015;309(1):L17–L26.
24. Bingle L, et al. BPIFB1 (LPLUNC1) is upregulated in cystic fibrosis lung disease. *Histochem Cell Biol*. 2012;138(5):749–758.
25. Park SW, et al. The protein disulfide isomerase AGR2 is essential for production of intestinal mucus. *Proc Natl Acad Sci USA*. 2009;106(17):6950–6955.
26. Bergström JH, Berg KA, Rodríguez-Piñeiro AM, Stecher B, Johansson ME, Hansson GC. AGR2, an endoplasmic reticulum protein, is secreted into the gastrointestinal mucus. *PLoS ONE*. 2014;9(8):e104186.
27. Podolsky DK, et al. Identification of human intestinal trefoil factor. Goblet cell-specific expression of a peptide targeted for apical secretion. *J Biol Chem*. 1993;268(9):6694–6702.
28. Wiede A, Jagla W, Welte T, Köhnlein T, Busk H, Hoffmann W. Localization of TFF3, a new mucus-associated peptide of the human respiratory tract. *Am J Respir Crit Care Med*. 1999;159(4 Pt 1):1330–1335.
29. Madsen J, Mollenhauer J, Holmskov U. Review: Gp-340/DMBT1 in mucosal innate immunity. *Innate Immun*. 2010;16(3):160–167.
30. Fu XW, Song PF, Spindel ER. Role of Lynx1 and related Ly6 proteins as modulators of cholinergic signaling in normal and neoplastic bronchial epithelium. *Int Immunopharmacol*. 2015;29(1):93–98.
31. Ohlmeier S, et al. Lung tissue proteomics identifies elevated transglutaminase 2 levels in stable chronic obstructive pulmonary disease. *Am J Physiol Lung Cell Mol Physiol*. 2016;310(11):L1155–L1165.
32. Recktenwald CV, Hansson GC. The Reduction-insensitive Bonds of the MUC2 Mucin Are Isopeptide Bonds. *J Biol Chem*. 2016;291(26):13580–13590.
33. Komi DE, Kazemi T, Bussink AP. New Insights Into the Relationship Between Chitinase-3-Like-1 and Asthma. *Curr Allergy Asthma Rep*. 2016;16(8):57.
34. Lee RM, Han KH, Han JS. rbCLCA1 is a putative metalloprotease family member: localization and catalytic domain identification. *Amino Acids*. 2016;48(3):707–720.
35. Bergström JH, et al. Gram-positive bacteria are held at a distance in the colon mucus by the lectin-like protein ZG16. *Proc Natl Acad Sci USA*. 2016;113(48):13833–13838.
36. Thornton DJ, Rousseau K, McGuckin MA. Structure and function of the polymeric mucins in airways mucus. *Annu Rev Physiol*. 2008;70:459–486.
37. Ridley C, et al. Assembly of the respiratory mucin MUC5B: a new model for a gel-forming mucin. *J Biol Chem*. 2014;289(23):16409–16420.
38. Ermund A, Schütte A, Johansson ME, Gustafsson JK, Hansson GC. Studies of mucus in mouse stomach, small intestine, and colon. I. Gastrointestinal mucus layers have different properties depending on location as well as over the Peyer's patches. *Am J Physiol Gastrointest Liver Physiol*. 2013;305(5):G341–G347.
39. Schütte A, et al. Microbial-induced meprin β cleavage in MUC2 mucin and a functional CFTR channel are required to release anchored small intestinal mucus. *Proc Natl Acad Sci USA*. 2014;111(34):12396–12401.
40. Bonser LR, Zlock L, Finkbeiner W, Erle DJ. Epithelial tethering of MUC5AC-rich mucus impairs mucociliary transport in asthma. *J Clin Invest*. 2016;126(6):2367–2371.
41. Lidell ME, Bara J, Hansson GC. Mapping of the 45M1 epitope to the C-terminal cysteine-rich part of the human MUC5AC mucin. *FEBS J*. 2008;275(3):481–489.
42. Zhu Y, et al. Munc13-2–/– baseline secretion defect reveals source of oligomeric mucins in mouse airways. *J Physiol (Lond)*. 2008;586(7):1977–1992.
43. van der Post S, Hansson GC. Membrane protein profiling of human colon reveals distinct regional differences. *Mol Cell Proteomics*. 2014;13(9):2277–2287.
44. Wiśniewski JR, Zougman A, Nagaraj N, Mann M. Universal sample preparation method for proteome analysis. *Nat Methods*. 2009;6(5):359–362.
45. Rappsilber J, Mann M, Ishihama Y. Protocol for micro-purification, enrichment, pre-fractionation and storage of peptides for proteomics using StageTips. *Nat Protoc*. 2007;2(8):1896–1906.
46. Cox J, Mann M. MaxQuant enables high peptide identification rates, individualized p.p.b.-range mass accuracies and proteome-wide protein quantification. *Nat Biotechnol*. 2008;26(12):1367–1372.
47. MacLean B, et al. Skyline: an open source document editor for creating and analyzing targeted proteomics experiments. *Bioinformatics*. 2010;26(7):966–968.